THE JOURNAL OF PHYSICAL CHEMISTRY B

 VOLUME 108, NUMBER 37, SEPTEMBER 16, 2004

ARTICLES

MoS_2 Nanostructures: Synthesis and Electrochemical Mg^{2+} Intercalation

Xiao-Lin Li and Ya-Dong Li*

Department of Chemistry, the Key Laboratory of Atomic & Molecular Nanosciences (Ministry of Education, China), Tsinghua University, Beijing, 100084, P. R. China

Received: September 15, 2003; In Final Form: July 13, 2004

MoS_2 nanostructures including hollow-cage fullerene-like particles, fibrous floccus, and spherical nanovesicles have been successfully synthesized by designed solution chemical reactions of Na_2MoO_4 and sulfurization reagents such as CS_2, Na_2S, CH_3CSNH_2, CSN_2H_4, and KSCN etc. Possible redox reaction routes have been proposed on the basis of the experimental facts. We have investigated the electrochemical properties of annealed MoS_2 samples finding that Mg^{2+} ions showed better reversibly intercalation/deintercalation cycles in as-synthesized MoS_2 nanostructures than in bluk MoS_2 samples. The solution product of MoS_2 and their high-temperature annealing samples were characterized by X-ray powder diffraction (XRD) and transmission electron microscopy (TEM), X-ray photoelectron spectroscopy (XPS), and resonance Raman spectra.

Introduction

Transition metal sulfides are a large family of materials that show many interesting properties such as superconductivity, fluorescence, electrical properties, and magnetism.[1−4] Among these compounds, MoS_2 has a layered structure, which consists of covalently bound S−Mo−S trilayers separated by a relatively large van der Waals gap.[5] Due to the distinctive layer structure and electronic properties, MoS_2 attracted considerable attention and has been investigated extensively as indispensable industrial catalysts for hydrodesulfurization of crude oil[6] and solid lubricants in high temperature and vacuum environments.[7] The weak interlayer interactions of MoS_2 also allow foreign atoms or molecules to be introduced between the layers through intercalation. Thus, MoS_2 could be developed as an intercalation host to form new materials[8] and a promising electrode material in high energy density batteries.[9−10] Recently, the requirement for cathode materials of rechargeable batteries has caused increasing interest in the intercalation of MoS_2. Tenne and co-workers have managed to intercalate alkali metals into fullerene-like MoS_2 nanoparticles and investigated the properties of these intercalation compounds.[8] Aurbach et al. have developed the rechargeable magnesium batteries using chevrel phase molybdenum sulfides as cathode materials.[10]

Nanosized materials with the novel morphologies were believed to have somewhat better performance than bulk materials. Tubular structured MoS_2 moieties have been found to display interesting electronic and optical properties that made them promising materials as probes for scanning probe microscopy techniques[11] and potential hydrogen storage media.[12] Recently, preparation of novel nanostructured MoS_2 and investigation of their electrochemical properties are attracting more and more interest. Various methods have been reported on the synthesis of nanosized MoS_2,[13−22] including the gas-phase reaction of MoO_3 and H_2S,[14] thermal decomposition of ammonium thiomolybdate,[15] and the solid-state reaction of $MoCl_5$ and Na_2S.[16] Sonochemistry, pulsed laser deposition, microwave irradiation, and hydrothermal reactions have also been developed to prepare nanosized MoS_2 at low temperature.[17−22] As-synthesized nanosized MoS_2 moieties showed good properties

* To whom all correspondence should be addressed. E-mail: ydli@tsinghua.edu.cn. Fax: (+86)-10-62788765.

10.1021/jp0367575 CCC: $27.50
Published on Web 08/21/2004

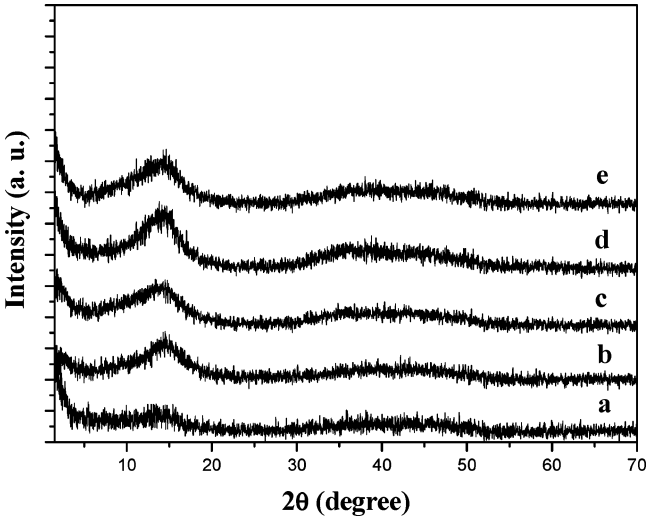

Figure 1. XRD patterns of MoS_2 obtained directly by the solution chemical reactions of (a) Na_2MoO_4 and CS_2, (b) Na_2MoO_4 and Na_2S, (c) Na_2MoO_4 and CH_3CSNH_2, (d) Na_2MoO_4 and CSN_2H_4, and (e) Na_2MoO_4 and KSCN.

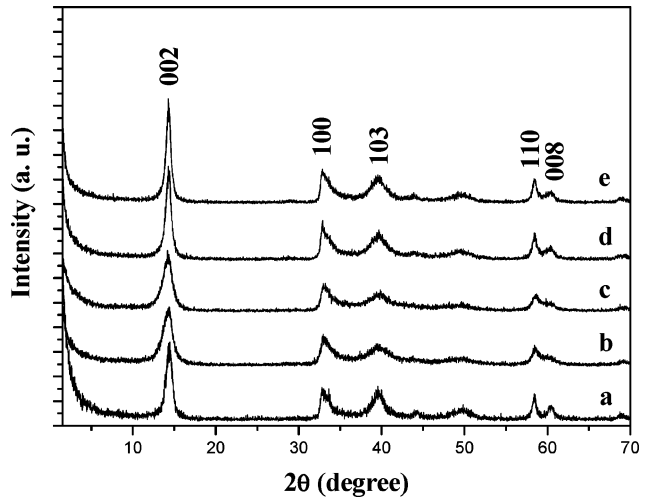

Figure 2. XRD patterns of annealed MoS_2 samples, which are prepared by the solution chemical reactions of (a) Na_2MoO_4 and CS_2, (b) Na_2MoO_4 and Na_2S, (c) Na_2MoO_4 and CH_3CSNH_2, (d) Na_2MoO_4 and CSN_2H_4, and (e) Na_2MoO_4 and KSCN.

and applications. In most of the reported reactions, reducing agents such as H_2 and $N_2H_4 \cdot H_2O$ were widely used for the synthesis of MoS_2. Since the low valent compounds of sulfur may serve as reductant in reactions, we believed that MoS_2 could be directly synthesized under appropriate conditions without using any additional reductant. Recently, we reported the synthesis of MoS_2 fullerene-like nanoparticles using the reaction of MoO_3 and S at moderate temperature.[23]

In this manuscript, we have designed several solution chemical reaction routes to prepare MoS_2 at low temperature. Some novel MoS_2 nanostructures, including hollow-cage fullerene-like nanoparticles, fibrous floccus, and spherical nanovesicles have been obtained. The possible reaction mechanisms were proposed according to the experimental results. This strategy provides an alternative route to synthesize nanosized MoS_2 at low temperature and is expected to open up a general method for the synthesis of other transitional metal dichalcogenides. Magnesium intercalation in annealed MoS_2 samples was investigated. Obvious charge−discharge cycles have been observed showing the possibility of MoS_2 in fabricating rechargeable magnesium batteries.

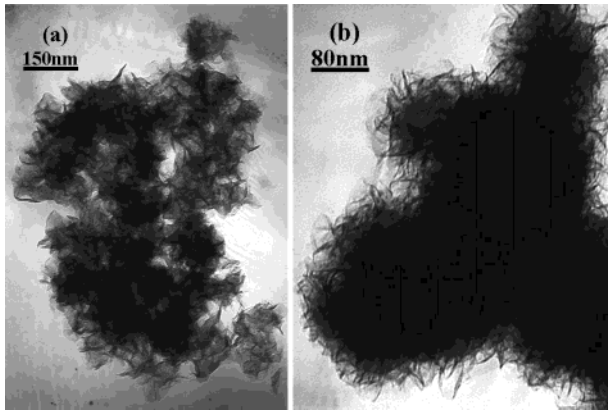

Figure 3. (a, b) TEM images of MoS_2 fibrous floccus obtained from the solution reactions of Na_2MoO_4 and CH_3CSNH_2.

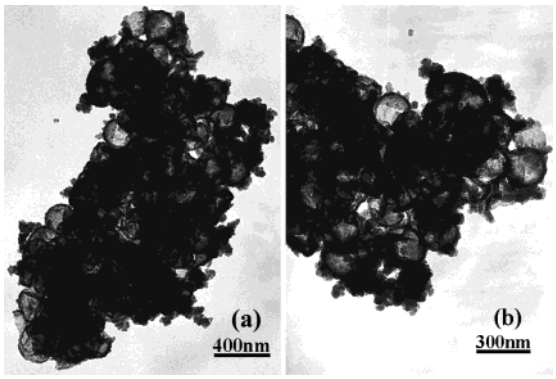

Figure 4. (a, b) Typical TEM images of spherical MoS_2 nanovesicles obtained from the reaction of Na_2MoO_4 and CH_3CSNH_2.

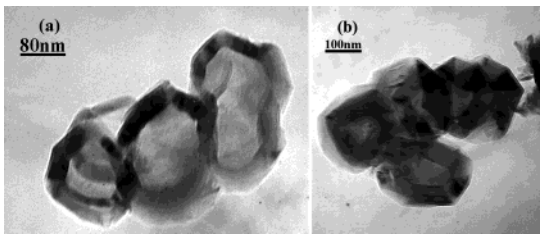

Figure 5. (a, b) Representative TEM images of MoS_2 fullerene-like nanoparticles obtained from the solution chemical reactions of Na_2MoO_4 and CH_3CSNH_2.

Experimental Section

Materials All chemicals used in this work, such as sodium molybdate (Na_2MoO_4), sodium sulfide (Na_2S), thioacetamide (CH_3CSNH_2), sulfocarbamide (CSN_2H_4), potassium sulfocyanide (KSCN), and carbon disulfide (CS_2) were analytical grade reagents.

Solution Synthesis of MoS_2. MoS_2 was successfully synthesized in solution-phase by the reaction of Na_2MoO_4 and several sulfurization reagents.

In a typical synthesis, 3 mmol of Na_2MoO_4 (about 0.73 g) and 9 mmol of sulfurization reagent were added into 30 mL of distilled water. Then 12 mol/L HCl was dropped into the solution while stirring to adjust the pH value to less than 1. The solution was transformed into a Teflon-lined stainless steel autoclave and heated at 180 °C for 24 h. After cooled to room temperature, the resulting precipitates of MoS_2 were filtered, washed with distilled water and dried in a vacuum at 80 °C for 12 h. Calcination treatment of as-synthesized MoS_2 samples was carried out in a conventional tube furnace at 700 °C with the argon flow rate of about 20 sccm (standard cubic centimeter

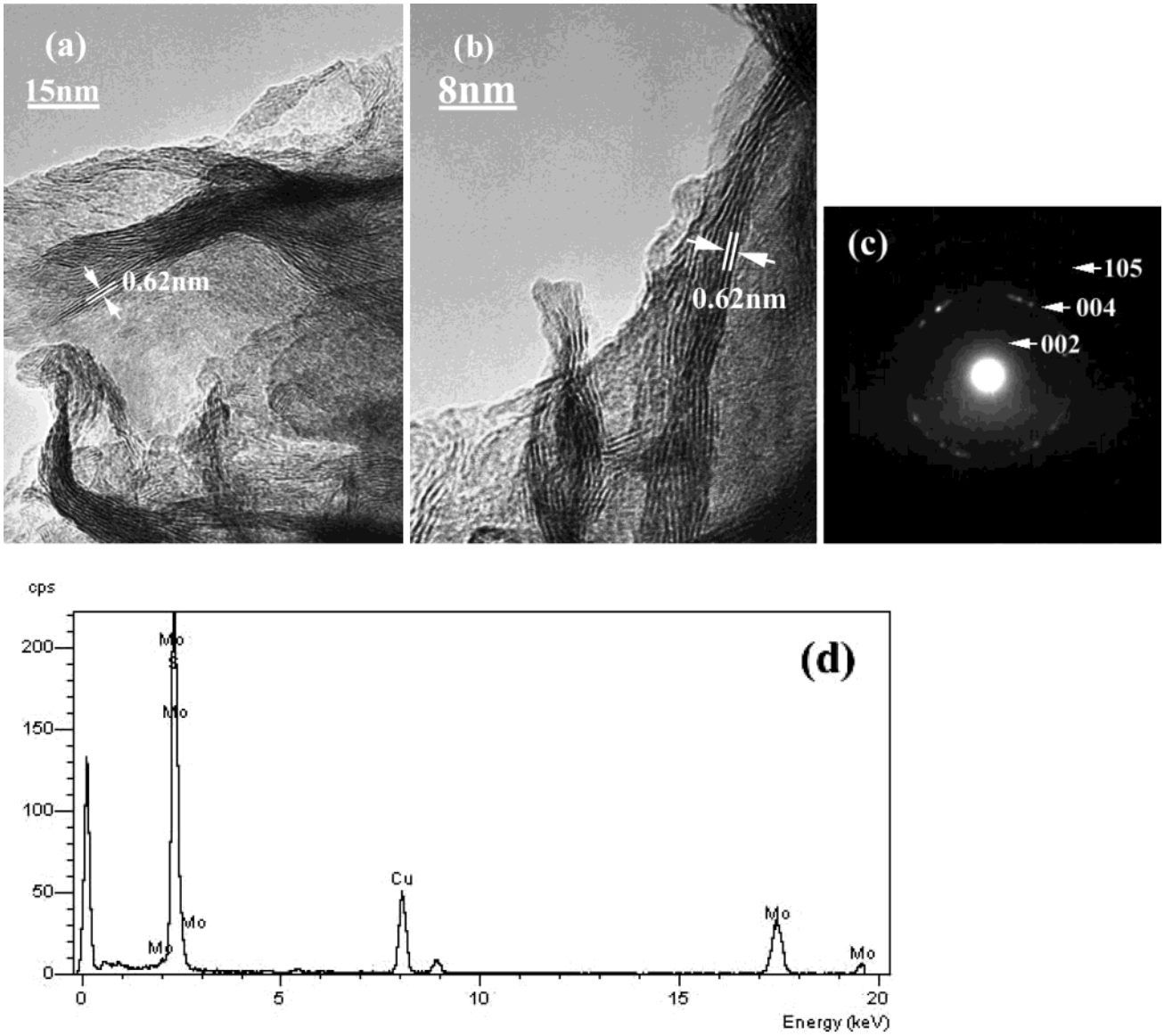

Figure 6. (a, b) HRTEM images of MoS_2 obtained from the solution reaction of Na_2MoO_4 and CH_3CSNH_2. The lattice fringes were about 0.62 nm, confirming that the product obtained by the solution chemical reaction was MoS_2. (c) Typical SAED pattern. (d) EDS spectrum.

per minute). Before the samples were heated, the tube was evacuated and purged to ensure the gas in the tube was normally pure argon.

Characterization

Powder X-ray diffraction (XRD) was performed on a Bruker D8-advance X-ray diffractometer with Cu Kα radiation (λ = 1.54178 Å). The 2θ range used in the measurement was from 1.5 to 70° in steps of 0.02° with a count time of 1 s. The samples were grind and placed on a glass substrate for XRD characterization. The size and morphology of all samples were determined by using a Hitachi model H-800 transmission electron microscopy (TEM), with a tungsten filament at an accelerating voltage of 200 kV. Lattice structures of the solution-products and their annealing samples were characterized by high-resolution transmission electron microscopy (HRTEM, JEOL-2010F). TEM specimens were prepared via the following procedure: the samples were dispersed in alcohol with the aid of 10 min ultrasonic vibration. Then a drop of the solution was transferred onto a standard holey carbon-covered-copper TEM micro grid. Raman spectra were taken under ambient condition by using a RM 2000 microscope confocal Raman spectrometer (Renishaw PLC., England). The spectrometer used the 632.8 nm line of a He−Ne laser at 17 mW of power, which was focused over the specimen on the order of 20 μm size with on-axis illumination and 90° backscattered Raman light collection. The scattered radiation was analyzed using an 1800 g/mm grating with an air-cooled 1024 × 256 pixel array CCD detector. A spectrum resolution of 1 cm^{-1} was obtained. A glass substrate was used as the sample holder.

Results and Discussion

XRD were used to determine the crystallinity and phase structure of the products. Figure 1 provided the typical XRD pattern of the samples obtained by the solution-phase reactions. As shown in the image, all of curves exhibited low and broad diffraction peaks. With the help of TEM results, the causes of the broad XRD peaks of the solution products were tentatively analyzed. According to the TEM results, the solution products were mainly small-sized crystallites and had a relatively wide size distribution. Large particles were in a small quantity. The crystallinity and strain in the crystallites could be found from

the TEM results of the unannealed products. Thus, the broad peak was believed to mainly occur by some combination of the small size particles, the disorder in the crystallinity, and the strain in the crystallites. Annealing had some effect on the crystal growth; thus, the annealed samples had more large-sized crystallites. The crystallinity of the products could be greatly increased by high-temperature treatment. Corresponding XRD patterns of the annealed samples (treated at 700 °C) are shown in Figure 2, in which all the reflections have been indexed to pure hexagonal MoS_2 with lattice constants $a = 3.161$ Å, $c = 12.299$ Å (JCPDS card No: 37-1492). The XRD data is analogous with that seen by Reznik using MoS_2 instead of graphite.[24] The peak positions for the sharp, symmetric 00*l* lines probably represent some sort of average lattice constant probing the interlayer spacing. The 100 and 101 peaks were not completely separated in the pattern; thus, sawtooth-shaped asymmetry reflections were found. Using least-squares methods (Metric, Bruker Company), we have also calculated the lattice constants from our actual data. The cell parameters were refined to be a hexagonal cell with $a = 3.155(2)$ Å, $c = 12.36(2)$ Å, which were close to those from the JCPDS card.

Hexagonal MoS_2 crystallites could be obtained only through heating at high-temperature, which has revealed that the initial product of solution-phase synthesis was nanosized MoS_2.

On the basis of TEM checking, products of all the designed reactions showed the analogous morphologies. Thus, we took the product obtained from the reaction of Na_2MoO_4 and CH_3CH_2SN as an example for TEM characterization.

Transmission electron microscopy (TEM) allowed the direct imaging of MoS_2 nanocrystals and provided much information on their structure. Representative TEM images of MoS_2 fibrous floccus are shown in Figure 3, parts a and b. As shown in the images, various MoS_2 thin layers folded and tangled together forming the fibrous morphology with wormlike grains. This might be ascribed to the large flexibility of MoS_2 planes for deformation. Another feature that was noticed was that the crystallinity of this kind of structure was poor. Their electron diffraction pattern showed very weak polycrystalline circles. Parts a and b of Figure 4 showed typical TEM images of spherical MoS_2 nanovesicles. Those nanovesicles usually had spherical geometries with diameters of about 200 nm. Because the vesicles had very thin walls, they might easily lose the regular spherical geometry and collapse into folded films or floccus. MoS_2 fullerene-like nanoparticles were usually obtained at high temperature of 850 °C. However, in this work, we found that they could be synthesized in the solution-phase at a rather low temperature. Parts a and b of Figure 5 showed the typical TEM images of MoS_2 fullerene-like nanoparticles obtained by the solution-phase reaction at 180 °C. Unlike the spherical fullerene-like nanoparticles obtained by Tenne et al. at high temperature, as-synthesized MoS_2 fullerene-like nanoparticles had a polygonal shape with a large diameter of about 150 nm.

HRTEM images provided further insight into the structure of the solution product of MoS_2. parts a and b of Figure 6 were the HRTEM images of MoS_2 obtained by the solution reaction of Na_2MoO_4 and CH_3CSNH_2. A crystal lattice could be seen clearly from those images. The lattice fringes were about 0.62 nm corresponding to the spacing between MoS_2 (002) basal planes. It indicated that the product obtained by the solution-phase reactions was MoS_2. The selected-area electron diffraction (SAED) pattern further confirmed that MoS_2 obtained by the solution-phase reaction had very poor crystallinity. Figure 6c was the typical SAED pattern, in which all the reflection circles were indexed. The poorly crystallized MoS_2 layers were very thin, and there might not be enough of them to fit the Bragg condition due to further tangling (considering the wavelength of the electron are much shorter than that of X-ray). Moreover, there might be some amount of amorphous products in the sample. Thus, their corresponding XRD pattern only showed a weak wide (002) peak at about 14.3°, while the TEM image showed the regular lattice spacing. Since the weak wide (002) peak at about 14.3° was coincident with the lattice fringes (about 0.62 nm) shown in HRTEM image, we believed that the XRD result was coincident with that of TEM. Figure 6d was the energy-dispersive X-ray spectra (EDS) of the solution product. The sample was composed of Mo and S with the elemental ratio of about 1:2.13 (The Cu signal arose from the copper grid.)

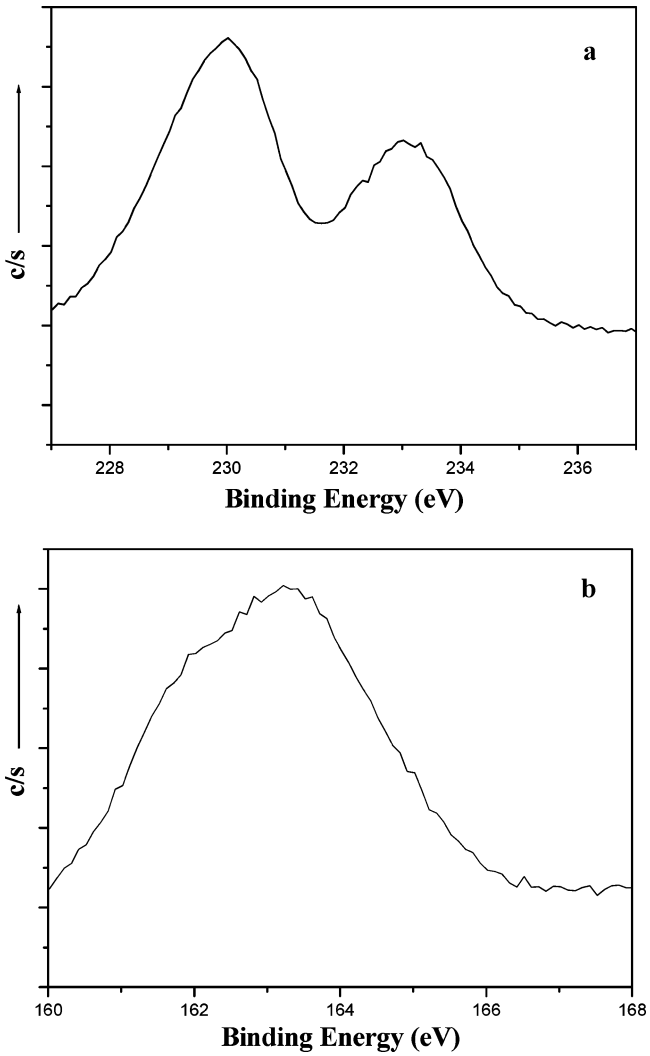

Figure 7. XPS spectra of the solution product obtained from the reaction of Na_2MoO_4 and CH_3CSNH_2: (a) Mo 3d spectrum (b) S 2p spectrum.

Since MoS_2 was stable in argon at elevated temperature, the thermal gravimetric analysis (TGA) showed no obvious weight loss. We have characterized the unannealed solution product using X-ray photoelectron spectroscopy (XPS) and Raman spectroscopy.

X-ray photoelectron spectroscopy (XPS, PHI-5300 ESCA) has been used to characterize the unannealed product. Parts a and b of Figure 7 showed the typical XPS spectra of the Mo 3d and S 2p, corresponding to the unannealed sample obtained by the reaction of Na_2MoO_4 and CH_3CH_2SN. In Figure 7a, the Mo $3d_{5/2}$ peak was located at 230.1 eV while the Mo $3d_{3/2}$ peak was at 233.1 eV. According to the literature,[18−19] these peaks

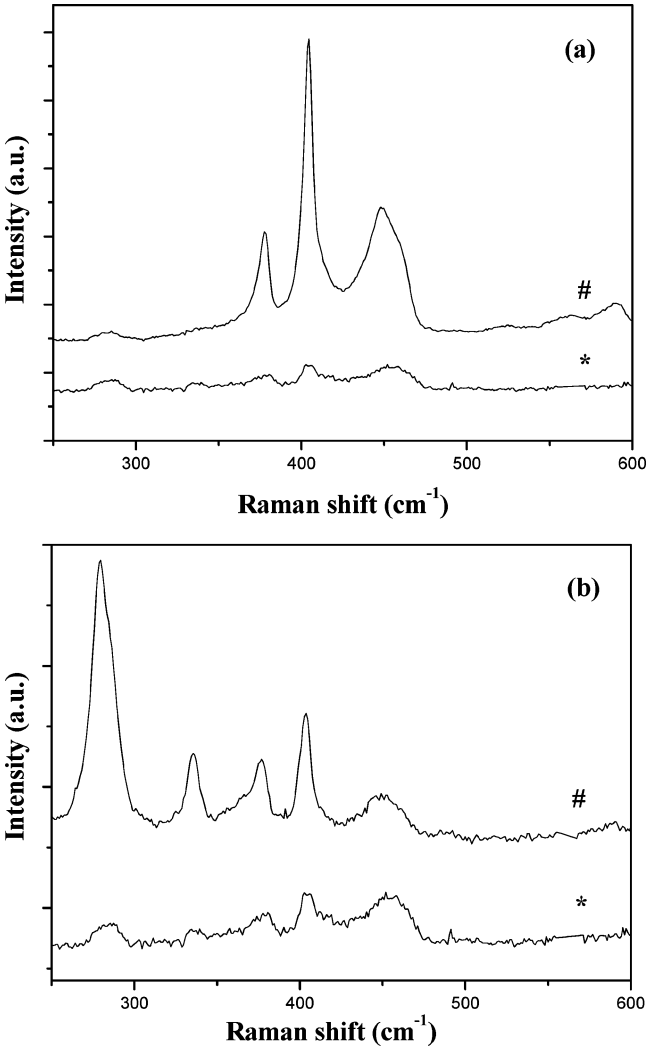

Figure 8. Raman spectra of (a) pure MoS_2 sample, and (b) partial oxidized MoS_2 sample: (∗) unannealed MoS_2 samples; (#) annealed MoS_2 samples.

could be attributed to Mo^{4+} atoms. In Figure 7b, S 2p spectrum primarily showed a strong XPS peak at 163.2 eV, which was ascribed to S^{2-}.[18−19]

Typical Raman spectra of the unannealed and annealed MoS_2 samples are shown in Figure 8a. With the wavelength used, the data obtained were resonance Raman. Although the peak intensities had great difference, the unannealed and annealed MoS_2 had the analogous peak positions at about 450, 405, 375, and 280 cm^{-1}, consistent with the literature.[25] We have measured the Raman spectra on many samples and all the spectra obtained were analogous. The relative intensities of the peaks changed with different samples and the reason was not sure. According to the literature,[25] normal Raman peaks of MoS_2 appeared at about 380 and 408 cm^{-1}. In the resonance Raman spectrum, besides the enhancement of those peaks at 405 and 375 cm^{-1}, some new peaks at about 450 and 280 cm^{-1} were obtained. In the measurement, if the laser power was too large and focused on the sample for a long time, the MoS_2 sample would be partially oxidized and a peak at about 340 cm^{-1} might appear. Figure 8b showed the Raman spectrum of partial oxidized MoS_2 sample. In Figure 8, parts a and b, all the corresponding peaks had analogous peak positions although the intensities were different.

Samples obtained from the solution-phase reactions were annealed at 700 °C for 2 h obtaining nanorods and fullerene-like nanoparticles. Typical TEM images of the annealed samples are shown in Figure 9, parts a and b. MoS_2 nanorods, platelets, and fullerene-like nanoparticles with sizes of about 100 nm could be seen clearly from those images. HRTEM images (Figure 10a,b) presented their regular lattice structure with a spacing of about 0.62 nm. A SAED pattern taken on an individual MoS_2 nanoparticle is shown in Figure 10c, in which all the diffractions have been indexed.

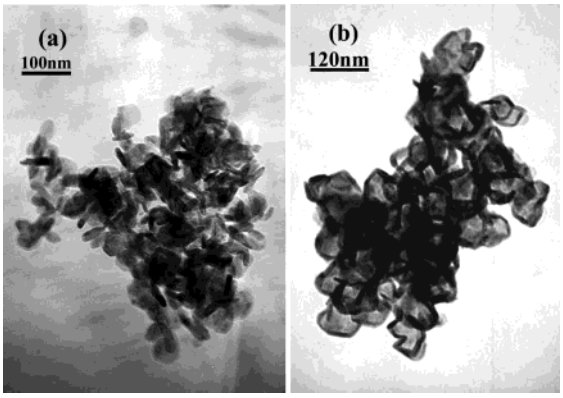

Figure 9. TEM images of MoS_2 obtained by annealing the solution product of Na_2MoO_4 and CH_3CSNH_2 at 700 °C: (a) MoS_2 platelet and nanorods; (b) MoS_2 fullerene-like nanoparticles.

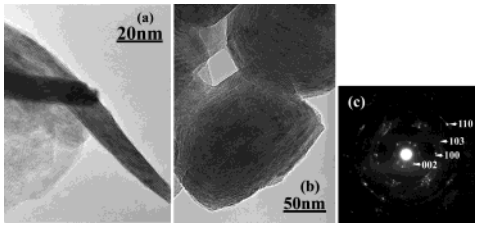

Figure 10. HRTEM images of MoS_2 nanorods and fullerene-like nanoparticles obtained by annealing the solution product of Na_2MoO_4 and CH_3CSNH_2 at 700 °C: (a) MoS_2 nanorods; (b) MoS_2 fullerene-like nanoparticles. (c) SAED pattern taken on individual MoS_2 fullerene-like nanoparticle.

Reaction Mechanism. It is well-known that Mo(VI) can be easily reduced in solution by reductant such as H_2, $NaBH_4$, SO_2, $N_2H_4{\cdot}H_2O$, and H_2S etc.[17−19,26] The sulfurization reagents such as CS_2, Na_2S, CH_3CSNH_2, CSN_2H_4, and KSCN, will easily decompose and form H_2S in acid solution at low temperature.[21,26] Thus, MoS_2 might be obtained by the reaction of Na_2MoO_4 and sulfurization reagents without using additional reductant. On the basis of the literature[17−19,26] and our experimental results, we believed that it was an oxidation−reduction process that should be responsible for the formation of MoS_2. In the reactions, sulfurization reagents also served as reductant. On the basis of the common knowledge concerning elemental sulfur and its compounds, the reaction routes for the synthesis of MoS_2 could be expressed as follows:

$$CS_2 + 2H_2O \rightarrow CO_2 + 2H_2S \quad (1)$$

$$Na_2S + 2HCl \rightarrow 2NaCl + H_2S \quad (2)$$

$$CH_3CSNH_2 + 2H_2O \rightarrow CH_3COONH_4 + H_2S \quad (3)$$

$$CSN_2H_4 + 2H_2O \rightarrow 2NH_3 + CO_2 + H_2S \quad (4)$$

$$KSCN + 2H_2O + HCl \rightarrow NH_3 + H_2S + CO_2 + KCl \quad (5)$$

$$4Na_2MoO_4 + 9H_2S + 6HCl \rightarrow 4MoS_2 + Na_2SO_4 + 12H_2O + 6NaCl \quad (6)$$

The overall reactions could be expressed as

$$8Na_2MoO_4 + 12HCl + 9CS_2 \rightarrow 8MoS_2 + 2Na_2SO_4 + 6H_2O + 12NaCl + 9CO_2 \quad (7)$$

$$4Na_2MoO_4 + 24HCl + 9Na_2S \rightarrow 4MoS_2 + Na_2SO_4 + 12H_2O + 24NaCl \quad (8)$$

$$4Na_2MoO_4 + 9CH_3CSNH_2 + 6H_2O + 6HCl \rightarrow 4MoS_2 + Na_2SO_4 + 9CH_3COONH_4 + 6NaCl \quad (9)$$

$$4Na_2MoO_4 + 9CSN_2H_4 + 6H_2O + 6HCl \rightarrow 4MoS_2 + Na_2SO_4 + 18NH_3 + 9CO_2 + 6NaCl \quad (10)$$

$$4Na_2MoO_4 + 9KSCN + 6H_2O + 15HCl \rightarrow 4MoS_2 + Na_2SO_4 + 6NaCl + 9NH_3 + 9CO_2 + 9KCl \quad (11)$$

Since hydrochloric acid was much excess in the reaction system, the formed NH_3 moieties actually were in the form of NH_4Cl. The pH value of the filtrate solution was detected to be about 1. Titrated with the mixed solution of $BaCl_2$ and HCl, the filtrate solution quickly became turbid and white precipitation of $BaSO_4$ was obtained. The existence of SO_4^{2-} provided strong evidence for our reaction routes.

There were a number of factors that might influence the reactions, such as the pH value, the reaction temperature, and the ionic intensities. Since most sulfurization reagents decomposed at temperatures higher than 150 °C, the synthesis of MoS_2 was carried out at 180 °C. Analogous to the reaction, other transitional metal dichalcogenides such as WS_2, and CdS have also been obtained. This strategy provided an alternative route to synthesize MoS_2 at low temperature, and was expected to open up a general method for the synthesis of other transitional metal dichalcogenides.

Electrochemical Mg^{2+} Intercalation. Among the numerous insertion/intercalation materials such as inorganic transition-metal oxides, sulfides, and borides proposed for positive electrodes of rechargeable batteries, transitional metal disulfides have attracted much attention recently.[9−10,27−32] Chemical and electrochemical intercalation of cations into two-dimensional layered transition metal disulfides of the general type MX_2 (M = Ti, Zr, Hf, Nb, Ta, Mo, W, V, and X = S) was well documented.[27−28] However, most of the work was devoted to the insertion of lithium and other alkali-metal ions into host materials.

Magnesium-based rechargeable batteries might be an interesting future alternative to lithium-based batteries, due to the high charge density, considerably negative electrode potential, natural abundance, less expense, environmental friendliness, and safety for handling.[10,29−30] However, in the development of rechargeable Mg batteries, the choice of the cathode material has been limited because it was difficult to achieve reversible Mg intercalation/deintercalation processes in many hosts. Recently, the intercalation of Mg^{2+} ions into transition metal sulfide based host structures has received increasing attention. Bruce et al. have investigated the chemical Mg^{2+} intercalation into TiS_2.[31] Aurbach et al. have developed Chevrel phase molybdenum sulfides as the cathodes for rechargeable magnesium batteries.[10] Novak and Desilvestro made a great step to carry out the electrochemical intercalation of Mg^{2+} into MoS_2 using a molten-salt electrolyte based on $MgCl_2/AlCl_3$/1-ethyl-3-methylimidazolium chloride (EMIC) at 80 °C.[32] Herein, we investigated the electrochemical properties of MoS_2 electrode and found that

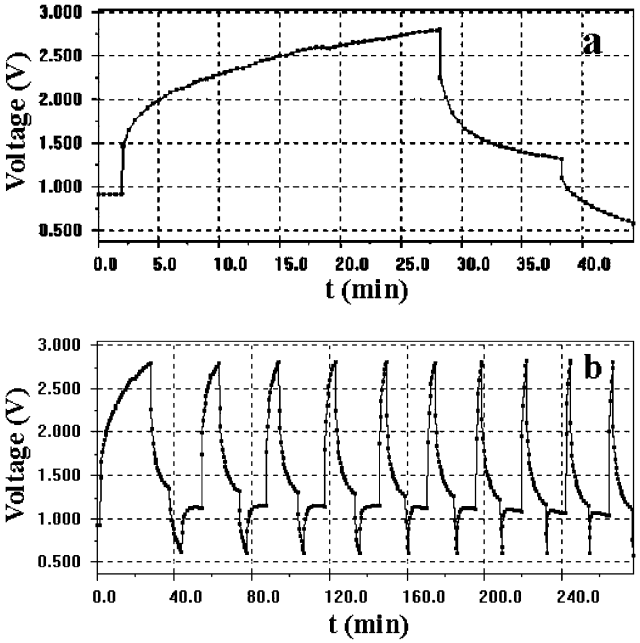

Figure 11. Electrochemical charge/discharge measurement of Mg/MoS_2 battery: (a) first charge/discharge curves of MoS_2; (b) ten complete cyclic charge/discharge curves of MoS_2. (The MoS_2 samples were prepared by calcination the solution product of Na_2MoO_4 and CH_3CSNH_2 at 700 °C for 2 h.)

Mg^{2+} ions might reversibly intercalate/deintercalate into our MoS_2 samples during the electrochemical charge/discharge processes.

In our experiments, Mg battery was comprised in a glovebox filled with pure argon using THF solution of $Mg(AlCl_3Bu)_2$ (Bu refers to butyl) as the electrolyte, Mg as the anode, and as-prepared annealing MoS_2 as the cathode. THF solution of $Mg(AlCl_3Bu)_2$ were prepared by ourselves. Ether solution of $MgBu_2$ and $AlCl_3$ were mixed in the ratio of. 1:2 and stirred at room temperature for 24−96 h. Then the solvent were evaporated and salt of $Mg(AlCl_3Bu)_2$ were obtained. Dissolving the magnesium salt in THF, a clear electrolyte solution was formed. Magnesium salt was stabilized in the solution by forming a kind of complex ion. It was the complex ions instead of solvated Mg^{2+} that act as the electric active cations in the electrochemical procedure. As-prepared annealed MoS_2 was fabricated as the cathode to examine the electrochemical properties. In each case, about 17 mg of MoS_2 were mixed with 2 mg of acetylene black powder and 1 mg of poly(tetrafluoroethylene) (PTFE) in slurry, pasted on to a nickel foam matrix, and then dried and pressed to construct a working electrode. Mg flakes were used as the counter and reference electrode. The Cellgard2400 was used as the membrane in the battery.

The charge−discharge measurements of Mg/MoS_2 cells were carried out on the Land battery measurement system at room temperature. Parts a and b of Figure 11 presented the constant current charge−discharge behavior of these batteries in terms of voltage vs time. The cell was cycled under constant current conditions, typically with a current of 0.05 mA (for charge) and 0.02 mA (for discharge) and cutoff voltage of 2.80 V (for charge) and 0.6 V (for discharge). Figure 11a was the first charge/discharge curve of the cell. As shown in the image, an obvious reversible charge/discharge phenomenon could be observed. Figure 11b showed 10 complete charge−discharge cycles of the battery. The fact that a large number of cycles could be repeated meant that the electrode structure did not breakup during the electrochemical procedure. We have carried

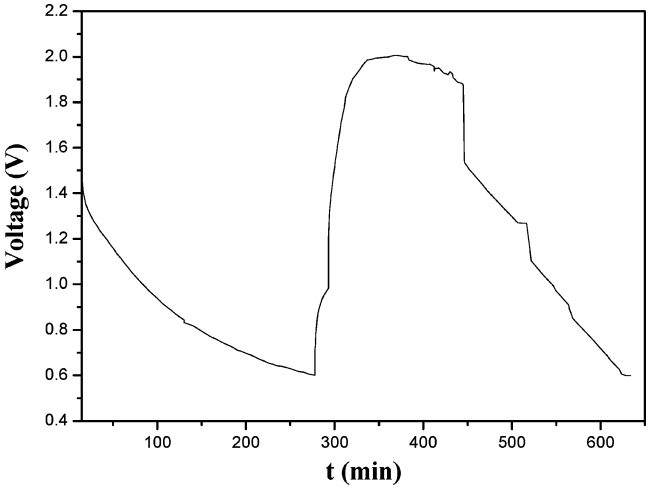

Figure 12. Electrochemical charge/discharge curve of another Mg/MoS_2 battery.

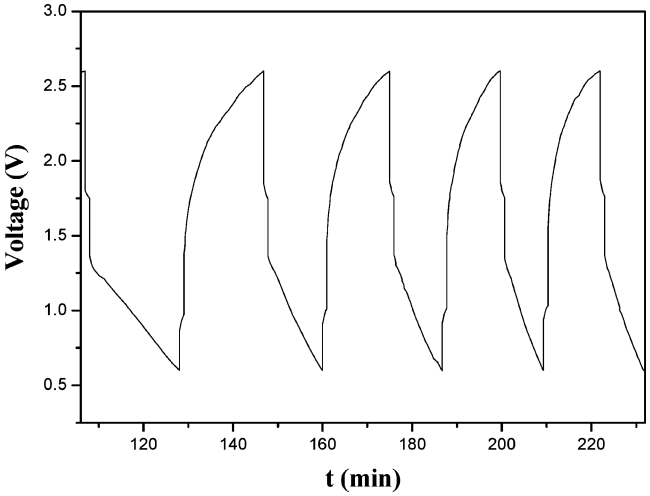

Figure 13. Control experiment of the electrochemical charge/discharge measurements using commercial MoS_2 powder.

out the charge/discharge measurements on many Mg/MoS_2 cells and found that the electrochemical behavior of the Mg/MoS_2 batteries such as the cell voltage, capacity, and efficiency showed small changes from one cell to another. This might due to the techniques are not well developed. However, we have found that in all the experiments, the batteries had the reversible charge/discharge cycling behavior, although the cyclic efficiency and capacity of our battery were low. Figure 12 showed the reversible charge/discharge curve of another cell, typically with a current of 0.05 mA (for charge) and 0.05 mA (for discharge) and cutoff voltage of 2 V (for charge) and 0.6 V (for discharge). Usually the capacity of the cell was about 2−25 mAh/g, and the discharge/charge efficiency was about 10−40%. The cell shown in Figure 11 had a capacity and efficiency of about 3 mAh/g and 25%, while the Mg/MoS_2 cell shown in Figure 12 had a capacity and efficiency of about 15 mAh/g and 38%.

After the intercalation experiments, we examined the MoS_2 cathode using TEM technique and did not find any obvious changes in the morphology of the sample. MoS_2 still showed the rod or fullerene-like nanostructure. We believed that this might be ascribed to the good crystallinity and relatively stable structure of the annealed samples.

Reversible intercalation/deintercalation of Mg^{2+} ions into MoS_2 has been successfully brought about by the electrochemical charge/discharge process. Although the detailed mechanism is not clearly understood at the present stage, a tentative explanation has been proposed. It was believed that the reversible intercalation of Mg^{2+} might be ascribed to several aspects: (1) No compact film of oxides were formed on magnesium (we have examined the surface of the Mg anode by XPS before and after intercalation and found that there were no oxides formed). Accompanying the adsorption phenomena, the reversible deposition/dissolution balance of Mg provided the possibility for the cyclic charge process.[28−30] (2) Magnesium would not only deposit and dissolve on the magnesium anode, but also had the reversible intercalation/deintercalation reaction happen on the MoS_2 electrode. We believed that it was the different size and nanostructure of MoS_2 that caused the different feature of the Mg^{2+} intercalation.[32] The MoS_2 nanorods and fullerene-like nanoparticles prepared by our method had small particle size and relative large amount of broken tips (as shown in Figure 9 and Figure 10), which might be suitable for ions intercalation. Moreover, *d* values between the layers of MoS_2 fullerene-like nanoparticles were slightly expanded because of the tension. This might also make it easy for the intercalation of Mg^{2+} ions.

Control experiment of electrochemical charge/discharge measurement using the commercial MoS_2 powders has been carried out. The commercial MoS_2 powder had an average particle size of about 400 nm based on the check of XRD and TEM. Strictly they were not bulk MoS_2. Since the commercial MoS_2 was the maximum sized MoS_2 we could get, we just used it as contrast to show the different charge/discharge behavior of different MoS_2 nanostructures. Figure 13 showed the charge/discharge curves of the electrode made of the commercial MoS_2 powders. As shown in the image, the charge/discharge process was usually fast and the curve was quite sharp. The voltage changed so quickly with time that the capacity of the cell was almost zero. Almost no Mg^{2+} was intercalated or deintercalated. Further investigation of the Mg/MoS_2 battery system is in progress.

The engineering of Li_xMnO_2, Li_xCO_2, MoO_3, V_2O_5 TiS_2, et al. into lithium cells are ongoing process, which has taken many decades. Engineering studies of cathodes into magnesium cells will be an ongoing process and may need more years for further investigation. The reversible intercalation of Mg^{2+} in MoS_2 may offer the possibility for preparing cathodes of transitional metal sulfides for Mg batteries.

Conclusion

In summary, we have developed several solution chemical reactions to synthesize MoS_2 at low temperature. Without using additional reductant, the reactions were much simplified. The redox reaction routes have been proposed on the basis of the experimental facts. Several MoS_2 novel nanostructures including hollow-cage fullerene-like nanoparticles, fibrous floccus, and spherical nanovesicles have been obtained. We investigated the electrochemical properties of MoS_2 electrode and found that Mg^{2+} ions might be reversibly intercalated/deintercalated into the annealed MoS_2 samples during the electrochemical charge/discharge processes.

Acknowledgment. We thank Prof. J. Chen, and Prof. H. T. Yuan for helpful discussions. This work was supported by the NSFC (20025102, 50028201, 20151001), the Foundation for the Author of National Excellent Doctoral Dissertation of P. R. China, and the State Key Project of Fundamental Research for Nanomaterials and Nanostructures.

References and Notes

(1) Matthias, B. T.; Marezio, M.; Corenzwit, E.; Cooper, A. S.; Barz, H. E. *Science* **1972**, *175*, 1465.

(2) Burlet, P.; Flouquet, J.; Genicon, J. L.; Horyn, R.; Pena, O.; Sergent, M. *Physica B* **1995**, *215*, 127.

(3) Zheng, D. N.; Ramsbottom, H. D.; Hampshire, D. P. *Phys. Rev. B* **1995**, *52*, 12931.

(4) (a) Wang, X.; Gao, P.; Li, J.; Summers, C. J.; Wang, Z. L. *Adv. Mater.* **2002**, *14*, 1732. (b) Peng, Z. A.; Peng, X. G. *J. Am. Chem. Soc.* **2001**, *123*, 183. (c) Li, Y. D.; Liao, H. W.; Ding, Y.; Qian, Y. T.; Yang, L.; Zhou, G. E. *Chem. Mater.* **1998**, *10*, 2301.

(5) (a) Dickinson, R. G.; Pauling, L. *J. Am. Chem. Soc.* **1923**, *45*, 1466. (b) Tenne, R. *Adv. Mater.* **1995**, *7*, 965.

(6) (a) Harris, S.; Chianelli, R. R. *J. Catal.* **1984**, *86*, 400. (b) Asudevan, P. T.; Fierro, J. L. G. *Catal. Rev.* **1996**, *38*, 161. (c) Zdrazil, M. *Appl. Catal.* **1982**, *4*, 107.

(7) (a) Chhowalla, M.; Amaratunga, G. A. J. *Nature (London)* **2000**, *407*, 164. (b) Rapoport, L.; Bilik, Y.; Feldman, Y.; Homyonfer, M.; Cohen, S. R.; Tenne, R. *Nature* **1997**, *387*, 791. (c) Rapoport, L.; Lvovsky, M.; Lapsker, I.; Leshchinsky, V.; Volovik, Y.; Feldman, Y.; Margolin, A.; Rosentsveig, R.; Tenne, R. *Nano Lett.* **2001**, *1*, 137.

(8) (a) Zak, A.; Feldman, Y.; Lyakhovitskaya, V.; Leitus, G.; Popovitz-Biro, R.; Wachtel, E.; Cohen, H.; Reich, S.; Tenne, R. *J. Am. Chem. Soc.* **2002**, *124*, 4747. (b) Remskar, M.; Skraba, Z.; Stadelmann, P.; Levy, F. *Adv. Mater.* **2000**, *12*, 814. (c) Homyonfer, M.; Alperson, B.; Rosenberg, Y.; Sapir, L.; Cohen, S. R.; Hodes, G.; Tenne, R. *J. Am. Chem. Soc.* **1997**, *119*, 2693.

(9) Imanishi, N.; Kanamura, K.; Takehara, Z. *J. Electrochem. Soc.* **1992**, *139*, 2082.

(10) (a) Aurbach, D.; Lu, Z.; Schechter, A.; Gofer, Y.; Gizbar, H.; Turgeman, R.; Cohen, Y.; Moshkovich, M.; Levi, E. *Nature (London)* **2000**, *407*, 724. (b) Lu, Z.; Schechter, A.; Moshkovich, M.; Aurbach, D. *J. Electroanal. Chem.* **1999**, *466*, 203. (c) Chusid, O.; Gofer, Y.; Gizbar, H.; Vestfrid, Y.; Levi, E.; Aurbach, D.; Riech, I. *Adv. Mater.* **2003**, *15*, 627.

(11) Rothschild, A.; Cohen, S. R.; Tenne, R. *Appl. Phys. Lett.* **1999**, *75*, 4025.

(12) Chen, J.; Kuriyama, N.; Yuan, H. T.; Takeshita, H. T.; Sakai, T. *J. Am. Chem. Soc.* **2001**, *123*, 11813.

(13) Li, Y. D.; Li, X. L.; He, R. R.; Zhu, J.; Deng, Z. X. *J. Am. Chem. Soc.* **2002**, *124*, 1411.

(14) (a) Tenne, R.; Margulis, L.; Genut, M.; Hodes, G. *Nature (London)* **1992**, *360*, 444. (b) Feldman, Y.; Wasserman, E.; Srolovitz, D. J.; Tenne, R. *Science* **1995**, *267*, 222. (c) Feldman, Y.; Frey, G. L.; Homyonfer, M.; Lyakhovitskaya, V.; Margulis, L.; Cohen, H.; Hodes, G.; Hutchison, J. L.; Tenne, R. *J. Am. Chem. Soc.* **1996**, *118*, 5362.

(15) (a) Zelenski, C. M.; Dorhout, P. K. *J. Am. Chem. Soc.* **1998**, *120*, 734. (b) Nath, M.; Govindaraj, A.; Rao, C. N. R. *Adv. Mater.* **2001**, *13*, 283.

(16) Bonneau, P. R.; Jarvis, R. F., Jr.; Kaner, R. B. *Nature (London)* **1991**, *349*, 510.

(17) Bezverkhy, I.; Afanasiev, P.; Lacroix, M. *Inorg. Chem.* **2000**, *39*, 5416.

(18) (a) Liao, H. W.; Wang, Y. F.; Zhang, S. Y.; Qian, Y. T. *Chem. Mater.* **2001**, *13*, 6. (b) Zhan, J. H.; Zhang, Z. D.; Qian, X. F.; Wang, C.; Xie, Y.; Qian, Y. T. *J. Solid State Chem.* **1998**, *141*, 270. (c) Li, W. J.; Shi, E. W.; Ko, J. M.; Chen, Z. Z.; Ogino, H.; Fukuda, T. *J. Cryst. Growth.* **2003**, *250*, 418.

(19) Chen, X. H.; Fan, R. *Chem. Mater.* **2001**, *13*, 802.

(20) (a) Lee, H.; Kanai, M.; Kawai, T. *Thin Solid Films* **1996**, *277*, 98. (b) Mosleh, M.; Laube, S. J. P.; Suh, N. P. *Tribol. T.* **1999**, *42*, 495.

(21) Mdleleni, M. M.; Hyeon, T.; Suslick, K. S. *J. Am. Chem. Soc.* **1998**, *120*, 6189.

(22) Vollath, D.; Szabo, D. V. *Mater. Lett.* **1998**, *35*, 236.

(23) Li, X. L.; Li, Y. D. *Chem.—Eur. J.* **2003**, *9*, 2726.

(24) Reznik, D.; Olk, C. H.; Neumann, D. A.; Copley, J. R. D. *Phys. Rev. B* **1995**, *52*, 116.

(25) Frey, G. L.; Tenne, R.; Matthews, M. J.; Dresselhaus, M. S.; Dresselhaus, G. *Phys. Rev. B* **1999**, *60*, 2883.

(26) (a) Greenwood, N. N.; Earnshaw, A. *Chemistry of the Elements*; Pergamon Press. Oxford, England, 1984. (b) Cotton, F. A.; Wilkinson, G.; Murillo, C. A.; Bochmann, M. *Advanced Inorganic Chemistry*; Wiley-Interscience: New York, 1999. (c) Shriver, D. F.; Atkins, P. W.; Langford, C. H. *Inorganic Chemistry*; Oxford University Press: Oxford, England, 1994.

(27) (a) Winter, M.; Besenhard, J. O.; Spahr, M. E.; Novak, P. *Adv. Mater.* **1998**, *10*, 725. (b) Pistoia, G., Ed. *Lithium Batteries. New Materials, Developments and Perspectives*; Elsevier, Amsterdam, 1994.

(28) (a) Chen, J.; Tao, Z. L.; Li, S. L. *Angew. Chem., Int. Ed.* **2003**, *42*, 2147. (b) Dominko, R.; Arcon, D.; Mrzel, A.; Zorko, A.; Cevc, P.; Venturini, P.; Gaberscek, M.; Remskar, M.; Mihailovic, D. *Adv. Mater.* **2002**, *14*, 1531.

(29) Morita, M.; Yoshimoto, N.; Yakushiji, S.; Ishikawa, M. *Electrochem. Solid-State Lett.* **2001**, *4*, 177.

(30) Gregory, T.; Hoffman, R.; Winterton, R. *J. Electrochem. Soc.* **1990**, *137*, 775.

(31) Bruce, P. G.; Krok, F.; Nowinski, J.; Gibson, V. C.; Tavakkoli, K. *J. Mater. Chem.* **1991**, *1*, 705.

(32) (a) Novak, P.; Imhof, R.; Haas, O. *Electrochim. Acta.* **1999**, *45*, 351. (b) Novak, P. Final project report for the Swiss Federal Office of Energy, Project No. EF-PROCC(91)018; Paul Scherrer Institute: Villigen, Switzerland, 1994.